Review

Modern fluorescent proteins: from chromophore formation to novel intracellular applications

Olesya V. Stepanenko,[1] Olga V. Stepanenko,[1] Daria M. Shcherbakova,[2] Irina M. Kuznetsova,[1] Konstantin K. Turoverov[1] and Vladislav V. Verkhusha[2]
[1]*Institute of Cytology of Russian Academy of Sciences, St. Petersburg, Russia*
[2]*Department of Anatomy and Structural Biology and Gruss-Lipper Biophotonics Center, Albert Einstein College of Medicine, Bronx, NY, USA*

BioTechniques 51:313-327 (November 2011) doi 10.2144/000113765
Keywords: PALM; STORM; STED; FRET; PAmCherry; mKate; two-photon microscopy

The diverse biochemical and photophysical properties of fluorescent proteins (FPs) have enabled the generation of a growing palette of colors, providing unique opportunities for their use in a variety of modern biology applications. Modulation of these FP characteristics is achieved through diversity in both the structure of the chromophore as well as the contacts between the chromophore and the surrounding protein barrel. Here we review our current knowledge of blue, green, and red chromophore formation in permanently emitting FPs, photoactivatable FPs, and fluorescent timers. Progress in understanding the interplay between FP structure and function has allowed the engineering of FPs with many desirable features, and enabled recent advances in microscopy techniques such as super-resolution imaging of single molecules, imaging of protein dynamics, photochromic FRET, deep-tissue imaging, and multicolor two-photon microscopy in live animals.

A broad range of fluorescent proteins (FPs) of different colors, as well as their engineered analogs, are currently used as fluorescent tags for bioimaging (1–4). A key feature of all FPs that has attracted enormous interest is their ability to self-generate the intrinsic chromophore from three amino acids at positions 65–67 (numbering is given according to *Aequorea victoria* GFP or avGFP) without requiring cofactors or enzymatic components (5). A rigid β-barrel shell comprising the protein matrix surrounds the chromophore to ensure this vital function (2,6). Protein folding provides the driving force in chromophore formation, correctly orienting crucial residues to catalyze and direct chromophore synthesis pathways. Spectral tuning of permanently fluorescent FPs, fluorescent timers (FTs), and optical highlighters is then achieved through modifying the extent of π-conjugation within the chromophore and interactions with surrounding amino acids while the β-barrel protects the chromophore from the environment and restricts its flexibility, thus preventing non-radiative deactivation. The accumulation of knowledge regarding the relationship between FP structure and optical properties has led to the direct manipulation of FP properties.

Undoubtedly, the discovery and cloning of avGFP and its relatives has advanced our understanding of basic biology. For example, the application of FPs and their engineered variants has facilitated routine monitoring of gene activation as well as the selective labeling and analysis of single proteins, cellular organelles, and even whole cells (7,8). Genetically encoded FP-containing biosensors based on the principle of FRET (fluorescence resonance energy transfer) have been widely adopted for the investigation of protein-protein interactions and other biologically relevant events occurring in living cells (1,9). In addition, a number of single FP-based biosensors also have been designed to sense many important properties of the cellular environment, including pH, ion flux, and redox potential (10–14). Another recent development and improvement is the discovery of FPs with light-modulated spectral properties, collectively termed photoactivatable fluorescent proteins (PAFPs), and FPs which emit in the far-red region and possess large Stokes shift. These FPs have enabled a number of new applications including multicolor super-resolution imaging in fixed and live cells (15,16), imaging of protein dynamics via multicolor Fluorescence Cross-Correlation Spectroscopy (FCCS) (17), accurate FRET imaging using photochromic FRET (pcFRET) (18), the development of dual FRET biosensors (19), deep-tissue imaging (20,21) and multicolor two-photon (2P) microscopy for visualization of cellular processes in living animals (22). Here we review our current understanding of FP structure and function as well as the use of FPs in various biological applications.

Fluorescent protein structure and function: Chromophore formation and conversion

The ability of FPs to emit visible light derives from the post-translational self-modification of three amino acids at positions 65–67 which result in chromophore formation (5). Among the three chromophore-forming amino

acids, only the glycine residue located at position 67 is absolutely conserved within all FPs. All naturally occurring GFP-like proteins possess a tyrosine residue at position 66. This tyrosine residue is believed to provide the proper oxidative chemistry during chromophore maturation and prevent undesirable side reactions, such as backbone fragmentation and hydrolysis, from occurring (23,24). Unlike the glycine at position 67, position 66 tolerates substitution with any aromatic amino acid, resulting in mature, but chemically distinct chromophores that emit light in the cyan/blue range of spectra (5). Despite attempts to improve the photochemical characteristics of these cyan/blue-emitting GFP homologs, blue-emitting FPs possessing a histidine at position 66 rather than a tyrosine exhibit low brightness in comparison to their green-emitting GFPs counterparts.

Amino acids at position 65 are highly diverse among the GFP-like proteins of different color; residues in this position affect the resulting chemical structure of the chromophore. The heterocyclic rings of His65, cyclized Lys65 or Thr65 are incorporated into the three-ring π-system of the mature chromophore in red and yellow/orange FPs (see next sections). Figure 1 summarizes the main steps of the blue, green, and red chromophore maturation pathways. Chromophore maturation is driven by protein folding which results in the proper orientation of the catalytic amino acids near the chromophore-forming tripeptide. In the next sections, we attempt to detail the critical steps in blue, green, and red color acquisition in permanently emitting FPs, PAFPs, and FTs, and discuss improved FP variants from these different classes currently recommended for practical applications (Table 1).

"Green" chromophore synthesis

The formation of the green chromophore in avGFP, as well as other green FPs, has been described in detail before. Briefly, green chromophore synthesis comprises three stages: (i) cyclization of the tripeptide to an α-enolate form (transformation A→B in Figure 1), (ii) oxidation to cyclic imine (transformation B→C in Figure 1), and (iii) dehydration of the Cα-Cβ bond of Tyr66 resulting in a mature GFP-like chromophore which is able to emit green light in a deprotonated (anionic) state (transformations C→D→E in Figure 1). Interested readers are referred to a review by Wachter et al. for further details (25). In its neutral form, the GFP-like chromophore is usually nonfluorescent, but can acquire bright green fluorescence when an excited-state proton transfer (ESPT) occurs. The equilibrium between the neutral and anionic forms of the chromophore can be shifted by directed evolution (26–28).

Several recently developed FPs possessing large Stokes shift (LSS FPs) have neutral chromophores in the ground state (structures K and D in Figure 1). Currently, LSS FPs of different colors are available, including green (19,28), yellow (19), and red (17, 22). The large Stokes shift of these proteins results from ESPT that transforms the excited neutral form of the chromophore to an emitting anionic form (21,22,29,30). It is desirable for any LSS FP to have only a neutral chromophore in its ground state. Otherwise it will be difficult to discriminate an LSS FP from its conventional FP analog in multicolor applications. Among red LSS FPs recently developed, LSSmKate1 and LSSmKate2 satisfy this requirement. They have single-peaked spectra with excitation at 463 nm and emission at 624 nm for LSSmKate1 and excitation at 460 nm and emission at 605 nm for LSSmKate2 (22). The other red LSS FP available, mKeima, in addition to the main absorption peak at 440 nm shows a minor absorption peak at 580 nm due to the presence of the anionic form of the chromophore (29). Structure studies uncovered the mechanism responsible for the stabilization of the chromophore predominantly in neutral form in the ground state (29–32). Carboxyl groups in the vicinity of chromophore are responsible for this. It is thought that in the ground state, the pK_a of carboxyl groups is lower than pK_a of the Tyr66 side chain hydroxyl of the chromophore, thus leading to carboxyl ionization and stabilization of the chromophore in the neutral form (29–32). From the ground state, the chromophore is then excited to the anionic, light emitting intermediate form. It was demonstrated that the ESPT pathway can be engineered in several conventional red-shifted FPs, including mNeptune, mCherry, mStrawberry, mOrange, and mKO, by introducing carboxyl groups in the vicinity of the chromophore (30), and the resulting mutants had large Stokes shifts. This opens the way for further development of missing LSS FP color variants, including orange and far-red, which will increase the number of FPs that could be imaged simultaneously in a cell. Development of spectrally well-separated orange and far-red LSS FPs would provide two additional LSS FPs spectroscopically distinct from each other and from existing green and red LSS FPs.

"Red" chromophore synthesis via blue intermediate

The red chromophore of the DsRed FP derived from *Discosoma* species and relatives represents an extended GFP-like core with an additional desaturated Cα-N bond at the Gln65 residue (structure L in Figure 1). An extended π-electron conjugation results in the red-shifted absorbance and emission (33). An early hypothesis whereby the maturation of the DsRed-like red chromophore proceeds via a green GFP-like chromophore (34) has been recently revised. According to current understanding, the maturation pathway of the DsRed-like red chromophore includes accumulation of a blue emitting intermediate (35,36) possessing a structure thought to be similar to the mTagBFP chromophore, a blue derivative of DsRed. Crystallographic and mass spectrometric analysis of mTagBFP revealed that the blue chromophore is composed of both a five-member ring and an N-acylimine double bond between Cα and N of Met65 (37) (structure J in Figure 1). The ring of the tyrosine residue at position 66 was shown to be nearly perpendicular to both the five-member imidazolone ring and acylimine group. Thus, exclusion of the phenolic ring from the chromophore π-conjugated electon system is responsible for the blue fluorescence of mTagBFP. According to Pletnev et al. (35), blue species form through oxidation of the α-enolate form (structure H in Figure 1), while in another model proposed by Strack et al. (36), the branch point in green/red chromophore formation is represented by the cyclic imine form (structure G in Figure 1). Here the second oxidation step with acylimine formation is in kinetic competition with the dehydration of the Cα-Cβ bond of Tyr66 to form the green chromophore. Conjugation of the blue mTagBFP-like chromophore with the phenolic ring of Tyr66 leads to the acquisition of red fluorescence in DsRed and relative red FPs.

The processes of chromophore maturation and conversion could be experimentally utilized in order to create FPs with new features. For example, the recently developed mCherry-based fluorescent timers (FT) take advantage of the time-delayed conversion of blue-

Table 1. Properties of improved fluorescent proteins

Protein	Ex_{max}[a] (nm)	Em_{max} (nm)	ε, $M^{-1}c_M^{-1}$	QY	Brightness[b]	pK_a	Structure	Additional parameter
Permanently fluorescent proteins								
								Maturation half time, h
EBFP2[1]	383	448	32,000	0.56	18	4.5	Monomer	0.42
Azurite[2]	383	447	26,200	0.55	14.4	5.0	Monomer	0.3
mTagBFP[3]	399	456	52,000	0.63	32.8	2.7	Monomer	0.22
TagCFP[4]	458	480	37,000	0.57	21.1	4.7	Monomer	ND
mTagGFP[4]	483	506	56,500	0.6	33.9	5.0	Monomer	0.18
TagYFP[4]	508	524	64,000	0.62	39.7	5.5	Monomer	ND
mKOκ[5]	551	563	105,000	0.61	64	4.2	Monomer	1.8
mOrange2[6]	549	565	58,000	0.60	34.8	6.5	Monomer	4.5
TagRFP-T[6]	555	584	81,000	0.41	33.2	4.6	Monomer	1.7
mRubby[7]	558	605	112,000	0.35	39.2	5	Monomer	2.8
LSSmKate2[8]	460	605	26,000	0.17	4.5	2.7	Monomer	2.5
mLumin[9]	587	621	70,000	0.46	32.2	4.7	Monomer	1.3
mKate2[10]	588	633	62,500	0.4	25	5.4	Monomer	<0.33
mNeptune[11]	599	649	57,500	0.18	10.4	5.8	Monomer	ND
eqFP650[12]	592	650	65,000	0.24	15.6	5.7	Dimer	ND
TagRFP657[13]	611	657	34,000	0,10	3.4	5.0	Monomer	2.0
eqFP670[12]	605	670	70,000	0.06	4.2	4.5	Dimer	ND
Fluorescent timers								
								Transition time[c], h
Slow-FT[14]	402 583	465 604	33,400 84,200	0.35 0.05	12 4	2.6 4.6	Monomer	9.8 28
Medium-FT[14]	401 579	464 600	44,800 73,100	0.41 0.08	18 6	2.7 4.7	Monomer	1.2 3.9
Fast-FT[14]	403 583	466 606	49,700 75,300	0.30 0.09	15 7	2.8 4.1	Monomer	0.25 7.1
mK-GO[15]	500 548	509 561	35,900 42,000	ND ND	ND ND	6.0 4.8	Monomer	10
Fluorescent proteins undergoing irreversible transitions								
								Condition[d]
PS-CFP2[16]	400 490	468 511	43,000 47,000	0.2 0.23	8.6 10.8	4.6 6.1	Monomer	initial state violet
PAmCherry1[17]	564	594	18,000	0.46	8	6.3	Monomer	violet
PATagRFP[18]	562	595	66,000	0.38	25	5.3	Monomer	violet
Dendra2[19]	490 553	507 573	45,000 35,000	0.50 0.55	22 19	6.6 6.9	Monomer	initial state violet
mEos2[20]	506 573	519 584	56,000 46,000	0.84 0.66	47 30	5.6 6.4	Monomer	initial state violet
mKikGR[21]	505 580	515 591	49,000 28,000	0.69 0.63	34 18	ND ND	Monomer	initial state violet
mIrisFP[22]	486 546	516 578	47,000 33,000	0.54 0.59	25 19	5.4 7.6	Monomer	violet (dark-to-green) cyan (red-to-dark) violet (green-to-red)
Fluorescent proteins undergoing reversible transitions								
								Condition of activation (quenching)[e]
mTFP0.7[23]	453	488	60,000	0.5	30	ND	Monomer	violet (458 nm)
Dronpa[24]	503	518	95,000	0.85	80.8	5.0	Monomer	violet (blue)
Padron[25]	503	522	43,000	0.64	27.5	ND	Monomer	blue (violet)
KFP1[26]	580	600	59,000	0.07	4.1	ND	Tetramer	green (450 nm)
rsTagRFP[27]	440 567	585 585	15,300 36,800	10^{-3} 0.11	0.02 4	ND 6.6	Monomer	orange blue

[a]Abbreviations: Ex_{max}, maximum of excitation spectrum; Em_{max}, maximum of emission spectrum; ε, molar extinction coefficient; QY, quantum yield. [b]The value of brightness is calculated as a product of quantum yield and molar extinction coefficient, divided by 1000. [c]Characteristic time for the color transition. [d]The condition of irreversible color transition. [e]The condition of reversible transition between fluorescent and dark states. [1] Ai et al., 2007. Biochemistry 46:5904–5910; [2] Mena et al., 2006. Nat. Biotechnol. 24:1569–1571; [3] Subach et al., 2008. Chem. Biol. 15:1116–1124; [4] www.evrogen.com; [5] Tsutsui et al., 2008. Nat Methods. 5:683–685; [6] Shaner et al., 2008. Nat Methods. 5:545–551; [7] Kredel et al., 2009. PLoS One. 4:e4391; [8] Piatkevich et al., 2010. Proc. Natl. Acad. Sci. USA. 107:5369–5374; [9] Chu et al., 2009. Biosens Bioelectron. 25:234–239; [10] Shcherbo et al., 2009. Biochem J. 418:567–574; [11] Lin et al., 2009. Chem. Biol. 16:1169–1179; [12] Shcherbo et al., 2010. Nat. Methods. 7:827–829; [13] Morozova et al., 2010. Biophys J. 99:L13–15; [14] Subach et al., 2009. Nat. Chem. Biol. 5:118–126; [15] Tsuboi et al., 2010. Mol. Biol. Cell. 21:87–94; [16] Chudakov et al., 2004. Nat. Biotechnol. 22:1435–1439; [17] Subach et al., 2009. Nat. Methods. 6:153–159; [18] Subach et al., 2010. J. Am. Chem. Soc. 132:6481–6491; [19] Gurskaya et al., 2006. Nat. Biotechnol. 24:461–465; [20] McKinney et al., 2009. Nat. Methods. 6:131–133; [21] Habuchi et al., 2008. PLoS One. 3:e3944; [22] Fuchs et al., 2010. Nat. Methods. 7:627–630; [23] Ai et al., 2006. Biochem. J. 400:531–540; [24] Ando et al., 2004. Science 306:1370–1373; [25] Andresen et al., 2008. Nat. Biotech. 26:1035–1040; [26] Chudakov et al., 2003. Nat. Biotechnol. 21:191–194; [27] Subach et al., 2010. Chem. Biol. 17:745–755.

to-red (38). FTs change their emission spectrum over time in a concentration-independent manner due to slow maturation of the chromophore. The predictable time course of color change from blue to red in the case of FTs can be used for quantitative analysis of temporal and spatial molecular events. In the cases of fast-FT, medium-FT, and slow-FT, the maxima of blue fluorescence is observed at 0.25, 1.2 and 9.8 h while the half-maxima of red fluorescence is reached at 7.1, 3.9, and 28 h, respectively. Key amino acids in the chromophore environment critical for the timing properties of FTs have been determined through the use of site-directed mutagenesis experiments. Amino acids Arg70 and Tyr83 have been shown to control Cα-Cβ double bond formation in Tyr66, while the presence of a serine residue at position 217 accelerates acylimine formation leading to faster blue chromophore formation. Ser146 also plays a crucial role in blue-to-red conversion by making the chromophore adopt a cis-configuration that is favorable for further oxidation (35).

In their resting states, photoactivatable FPs such as the PAmCherries are non-fluorescent, but will exhibit bright red fluorescence following UV-violet light illumination (15). According to crystallographic and mass spectrometric data, in the "dark-state" the PAmCherry1 chromophore adopts a non-planar configuration similar to the structure of the mTagBFP chromophore with N-acylimine functionality and a single non-oxidized Cα-Cβ bond at Tyr66 in the cyclized Met65-Tyr66-Gly67 tripeptide. After photon absorption, the excited mTagBFP-like PAmCherry1 chromophore is thought to accept an electron from the carboxyl group of Glu222 and release a CO_2 molecule via a Kolbe-like radical reaction (39). This decarboxylation of the Glu222 residue leads to the oxidation of the Tyr66 Cα-Cβ bond and subsequent red fluorescence acquisition (15).

Reversible and irreversible photoconversion of "red" and "green" chromophores

Decarboxylation of the Glu222 residue has also been observed in the irreversible dark-to-green photoactivation of PA-GFP (40) as well as in the cyan-to-green photoconversion of PS-CFP and PS-CFP2 (41). Both proteins possess the same chromophore-forming tripeptide motif, Ser65-Tyr66-Gly67, resulting in a neutral form of the GFP-like chromophore in the absence of UV-violet light (structure O in Figure 1). Light-induced decarboxy-

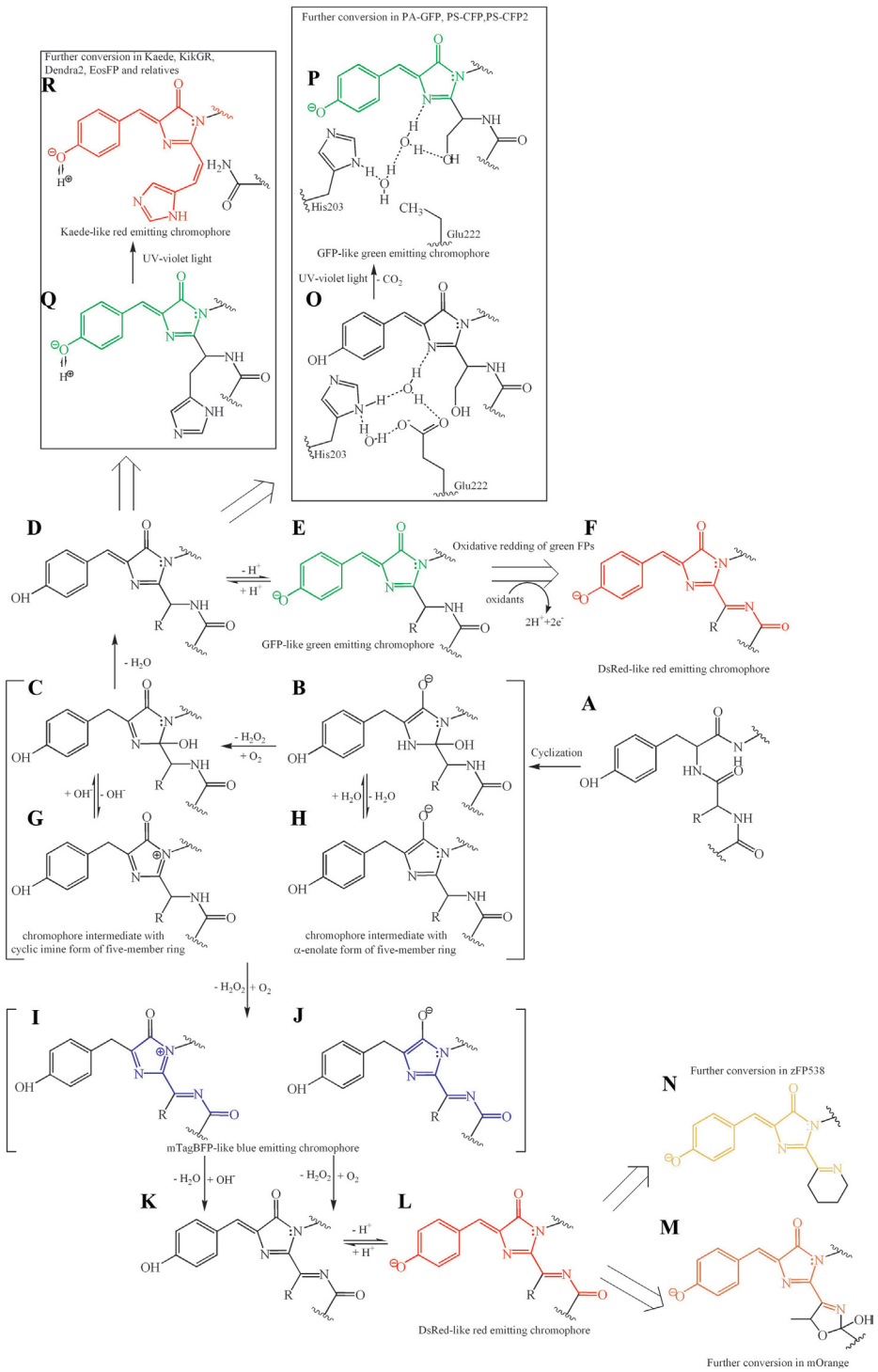

Figure 1. Chromophore formation pathways in the fluorescent proteins. A⟶B⟶C⟶D⟶E denotes the green chromophore formation pathway. A⟶B⟶H⟶J⟶K⟶L and A⟶B⟶C⟶G⟶I⟶K⟶L are two alternative pathways for red chromophore formation. L⟶N is the zFP538 chromophore formation pathway. L⟶M is the mOrange chromophore formation pathway. O⟶P is the light induced green-emitting chromophore formation pathway in the PA-GFP, PS-CFP and PS-CFP2 proteins. D⟶E⟶F is the oxidative redding pathway in the green FPs. Q⟶R is the light-induced chromophore transformation in the Kaede-like FPs.

lation of the Glu222 carboxyl group leads to a rearrangement of the chromophore environment, shifting the chromophore equilibrium to the anionic green emitting form (structure P in Figure 1) (42).

A totally different mechanism underlies the irreversible green-to-red photoconversion of the Kaede sub-family of FPs, which include Kaede, EosFP, DendFP and its engineered monomeric version Dendra2, mcavRFP, rfloRFP, mIrisFP, mEos2 and mKikGR (43,44). All proteins in the Kaede sub-family share the same chromophore-forming tripeptide motif, His65-Tyr66-Gly67, wherein the histidine residue at position 65 is critical to red fluorescence acquisition since substitution at this position with any other amino acid abolishes the green-to-red conversion. Non-activated Kaede-like proteins bear a two-ring chromophore in the cis-configuration, identical to the green chromophore of avGFP (structure Q in Figure 1). In the ground state, Kaede-like proteins show absorption spectra with two bands corresponding to the anionic and neutral forms of the GFP-like non-activated chromophore. Excitation of the neutral form triggers a series of photochemical events that results in backbone cleavage between the N-Cα atoms of His65 and formation of a Cα-Cβ double bond in His65 (structure R in Figure 1) (43). The final red-emitting chromophore comprises a three-ring system that undergoes reversible protonation-deprotonation between the non-fluorescent neutral form and fluorescent anionic form.

Green FPs of diverse origin can also undergo another type of photochemical reaction known as oxidative redding (transformation E→F in Figure 1) (45). Here the green-to-red photoconversion is driven by intense blue light (488 nm). The green FP chromophore in the excited state can donate electrons to appropriate electron acceptors in the vicinity, such as FAD, NAD+, flavins, and cytochromes, resulting in two-electron oxidation and most likely a DsRed-like chromophore.

Reversible photoconversion between a non-fluorescent OFF state and a fluorescent ON state has been observed for FPs of different colors. Among the FPs possessing this behavior are cyan mTFP0.7, green Dronpa, red asFP595 and its KFP derivative, rsCherry and rsCherryRev, green and red forms of IrisFP, red rsTagRFP (46,47). Some of these FPs, including mTFP0.7, Dronpa, rsCherryRev, IrisFP, are fluorescent in their resting, thermodynamically stable state but undergo quenching upon illumination with the light of a specific wavelength. The other FPs, including asFP595 and KFP, rsCherry, and rsTagRFP, are non-fluorescent in the absence of light but turn to the short-lived fluorescent state upon illumination. This state can relax back spontaneously or as the result of illumination at a different wavelength. It has been proposed that this photoconversion mechanism involves a light-induced cis-trans isomerization of the chromophore along with associated structural rearrangements within the chromophore's pocket and alterations of the hydrogen-bond network leading to a shift in the protonation/deprotonation equilibrium of the chromophore. Indeed, absorbance spectra of FPs in resting and photoconverted state indicate that the photoconversion process occurs concomitantly with changes in the protonation status of the chromophore (47–49). The increased flexibility and deviation in the planarity of the neutral chromophore is thought to be an efficient pathway for nonradiative dissipation of excitation energy.

Further post-translational modifications of acylimine which result in the formation of a tricyclic chromophore structure have been proposed to be responsible for spectral tuning in yellow/orange FPs. For example, cyclization of lysine at position 65 in the chromophore-forming tripeptide yields an additional tetrahydropyridine ring in yellow zFP538 FP (transformation L→N in Figure 1) (50), while the chromophore of mOrange contains an additional unusual dihydroxyoxazole ring derived from Thr65 (transformation L→M in Figure 1) (51). Less effective charge delocalization in these heterocyclic structures as compared with acylimine explains the hue of emission.

Bathochromic shift of emission in far-red and near-infrared FPs has also been proposed through additional interactions between the chromophore and its environment rather than chemical modification of the chromophore structure (20,21). However, we assume that additional chemical modifications could result in new versions of far-red shifted FPs.

Intracellular applications of fluorescent proteins

In recent years, a wide range of spectroscopic features have been realized for FPs through the application of directed evolution to available variants. Emerging imaging approaches and methods are tightly linked to the development of relevant fluorescent probes. As discussed above, understanding the maturation scheme of the FP chromophore and the peculiarities of its interaction with the surrounding β-barrel enables the generation of novel FPs which can be applied to modern techniques. In the next sections we briefly consider the latest advances in imaging techniques that rely on newly created FPs (see Figure 2).

Super-resolution techniques

Recently developed imaging approaches that break the diffraction limit can be divided into two categories (52,53). The first group of techniques achieves super-resolution through the narrowing of a fluorescent spot of an ensemble of many fluorophores using the spatial modulation of transitions between two molecular states. This group includes STED (stimulated emission depletion) (54), GSD (ground-state depletion) (55), and SSIM (saturated structured illumination microscopy) (56). The second approach for super-resolution imaging relies on single-molecule detection through the repeated switching on of sparse molecules to define their precise location and then subsequently reconstruct a super-resolution image. This group of techniques is represented by STORM (stochastic optical reconstruction microscopy) (57)

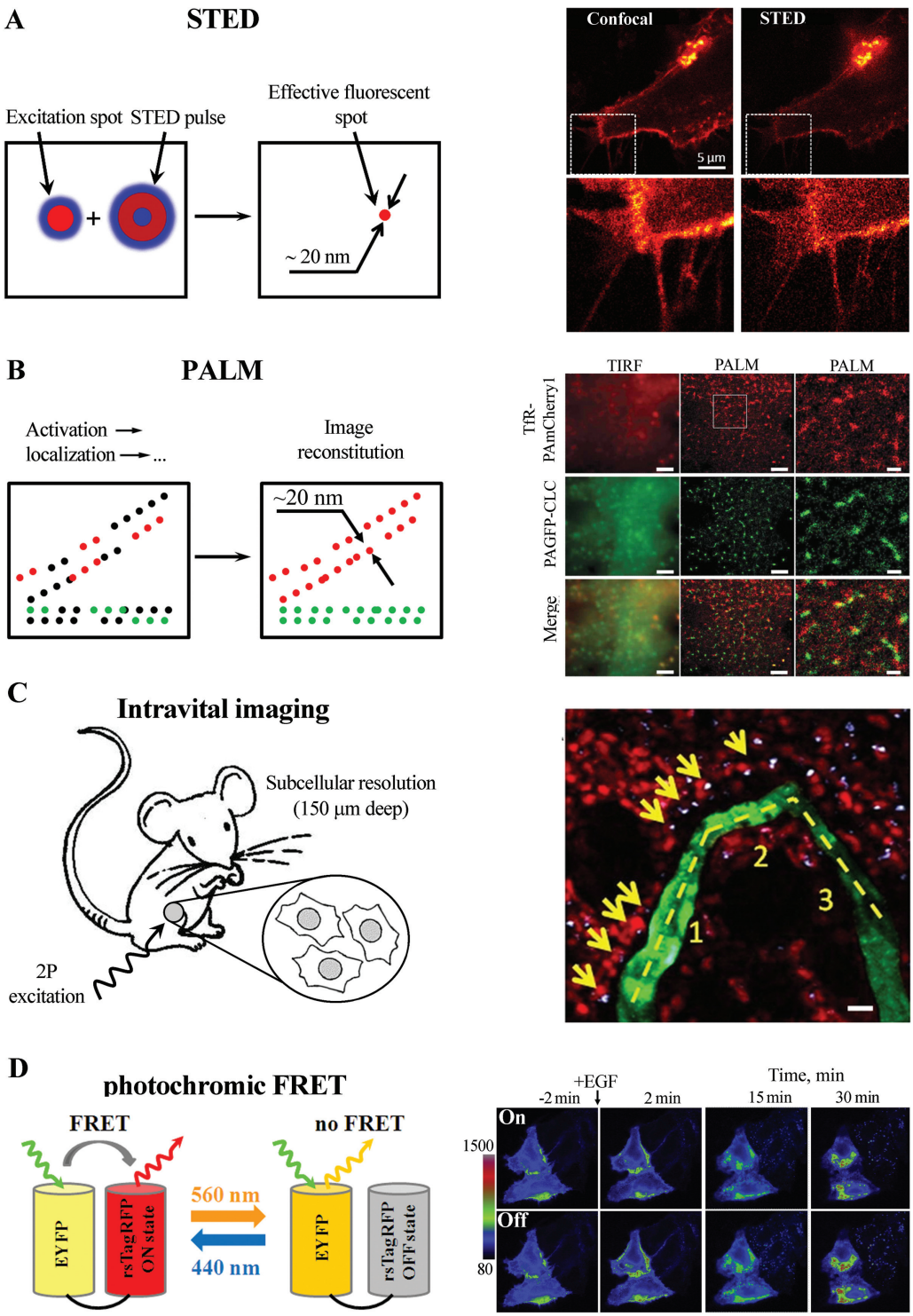

Figure 2. Advanced imaging techniques based on recently developed fluorescent proteins. (A) Schematic representation of STED microscopy (left panel) and the fine details of filopodia at the edge of the fixed HeLa cell revealed by STED microscopy (right panel, (68)). STED microscopy is based on the narrowing of an initial diffraction-limited excitation spot by applying a doughnut-shaped depletion laser pulse (STED pulse). The depletion results in an effective fluorescent spot of up to 20 nanometers in diameter. (B) Schematic representation of PALM microscopy (left panel) and application of two-color PALM microscopy for studies of colocalization of TfR tagged by PAmCherry1 and CLC tagged by PAGFP (right panel, (15)). PALM is based on a processing of the stack of images obtained by repeated activation of well-separated photoactivatable molecules, their localization using 2D Gaussian reconstruction, and subsequent bleaching. The resulting reconstituted image of the Gaussian centers provides a resolution of up to 20 nanometers. (C) Intravital imaging scheme relying on far-red/infrared FPs or far-red LSS-FPs and multiphoton excitation allowing subcellular resolution up to 150 µm in deep (left panel) and studies of tumor cell motility by 2P microscopy (right panel, (22)): the image of MTLn3 cells with stable coexpression of NLS-LSS-mKate1 (nucleus, red) and GalT-ECFP (Golgi, blue), and blood vessel labeled by FITC-dextran (green). (D) Photochromic FRET (pcFRET) scheme (left panel) and imaging of interaction between EGFR tagged with EYFP and Grb2 tagged with rsTagRFP in live HeLa cells using pcFRET (right panel, (18)) are shown. pcFRET is a technique for studying protein-protein interaction using the repeated switching on and off of the FRET process. The fluorescence emission of the FRET donor such as EYFP is modulated by the light-induced changes of absorbance spectrum of the rsTagRFP acceptor in its on and off states.

and PALM (photoactivated localization microscopy) (58). Here, FPs with irreversible or reversible light-induced phototransitions can be used to obtain high-resolution images of biological samples (59). The spatial and temporal resolution of these different super-resolution techniques depends on both the number of photons collected from each protein per unit time and the level of background noise arising from sample autofluorescence as well as any residual fluorescence from surrounding molecules when they are turned off. It should be noted that many available PAFPs still suffer from low brightness, although the largest fluorescence contrast and the highest photon output are provided by green-to-red photoswitchable EosFP (60), dark-to-red PAmCherries (15), and PATagRFP (16).

Since their development, all super-resolution imaging methods have successfully addressed different biological problems. PALM has been used to describe protein heterogeneity in the plasma membrane of live cells (61,62), determine the mobility dynamics of cytoskeletal proteins (63) and define the movement of individual actin molecules within live spines (64). Three-dimensional SSIM has enabled the accurate measurement of cellular structures such as replication foci (65) as well as the observation of several new features of mammalian nuclei (66). Researchers have used STED to study new aspects of synaptic vesicle recycling (67) and observe individual structural elements of microtubules, mitochondria, and other components of fixed cells (68) (Figure 2A) as well as the endoplasmic reticulum of living cells (69).

Advancements in multicolor super-resolution techniques, aided by the growing number of new FPs, has enabled studies of interacting species in a cell with a high precision. Two-color PALM has been successfully used to study adhesion complexes at super-resolution (70) as well as study the co-localization of the transferrin receptor (TfR) with clathrin light-chain (CLC) molecules (15,16) (Figure 2B). In the latter study, the authors generated two chimeras: TfR-PAmCherry1 and CLC-PAGFP. Different relative distributions of structures enriched in TfR-PAmCherry1 and CLC-PAGFP were identified and proposed to represent stages of clathrin-coated pit dynamics. These stages are: (i) mature clathrin-coated pits with CLC-PAGFP clusters and without TfR-PAmCherry1 cargo, (ii) mature uncoated vesicles close to the plasma membrane with TfR-PAmCherry1 clusters and without CLC-PAGFP, and (iii) early pits that have captured the TfR-PAmCherry1 cargo with the two proteins colocalized. It should be noted that the absence of a green emission state for PAmCherry1 enables greater flexibility when this FP is employed in one and two-color PALM experiments. In addition, the smaller size of the protein relative to tdEosFP is also advantageous as PAmCherry1 is potentially less disruptive to tagged fusion partners.

In comparison to PAmCherry1, monomeric PATagRFP displays even more advantages, including better pH stability, 3-fold higher brightness, and better photostability (16). The lack of a green emission state and lower efficiency of photoactivation with blue light makes PATagRFP an excellent protein tag for use in the super-resolution technique of single-particle tracking PALM (sptPALM). Chimeras of PATagRFP with different trans-membrane proteins (TfR, EGFR, and vesicular stomatitus virus G protein (VSVG)) used in concert with CLC tagged with PAGFP have performed well in two-color sptPALM. These experiments confirmed colocalization of those trans-membrane proteins with plasma membrane domains enriched in CLC, which are internalized into the cell via endocytosis.

An important consideration when performing any super-resolution imaging technique is the labeling density of fluorescent probe in the sample (53,71). When a higher labeling density is used, better effective resolution can be reached. However, at high densities of fluorescent probe, the contrast decreases even with the best FPs.

The performance of super-resolution techniques that rely on single-molecule localization such as PALM and STORM depends critically on the label used and the biological structure being imaged (53,71). These methods work better for imaging smaller filamentous objects than dense cellular structures. To enhance resolution, the signal should be detected from fewer fluorophores in smaller volume. However, this will lead to a drop in brightness. To compensate for this decreased brightness, more intense illumination is required, which is why molecular brightness and molecular photostability of a fluorescent probe are critical features for good performance in super-resolution techniques.

One current limitation of super-resolution techniques based on spatial patterning of the excitation light such as STED and SSIM is that these techniques require power levels that lead to bleaching of fluorescent probes (72). Thus, more photostable FPs are advantageous here. An additional consideration when choosing a probe for STED is that it should not be excited completely by the wavelength of light used for the depletion laser. The recently developed far-red monomeric FP TagRFP657 (68) has demonstrated good performance for use with the commercially available STED microscope system.

Intravital imaging

Deep-tissue imaging in living animals is of great interest as the technique can be applied to a range of questions in areas including oncogenesis, embryogenesis, and neurobiology. Here, experiments have been greatly facilitated through the development of far-red

and near-infrared emitting FPs since both autofluorescence and light scattering decrease substantially in living tissues when increased of wavelengths of light are used for excitation and emission. Several far-red shifted FPs are available today that can be used for in vivo cell-labeling, including E2-Crimson (73), mNeptune (21), TagRFP657 (68), eqFP650, and eqFP670 (20). The recently developed FPs eqFP650 and eqFP670 are characterized by fast maturation with no residual short-wavelength fluorescence from intermediate chromophore forms, in contrast to mNeptune and E2-Crimson. These FPs also show low cytotoxicity, which is crucial for whole-body imaging experiments. Injection of HEK 293T cells expressing E2-Crimson, mNeptune, eqFP650, and eqFP670 has been used to obtain whole-mouse images, with eqFP650 having the highest fluorescence. It was shown that eqFP650 had the highest emission when excited using 570/30 and 605/30 nm filters. However, no cell implants were visible in the infrared range under illumination at 640 nm, most probably owing to insufficient brightness at this excitation wavelength. At the same time, injection of test proteins subcutaneously into a living mouse to achieve higher local protein concentrations has provided comparable infrared signal from all proteins. At present, the dimeric nature of eqFP650 and eqFP670 prevent their application as fusion constructs. The far-red TagRFP657 (68), with monomeric behavior but lower brightness, performs well in intravital visualization of tumors in mice.

Another approach for deep penetration into live tissues is through the use of 2P excitation (74). The advantage of 2P microscopy is negligible out-of-focus photobleaching and photodamage incurred by surrounding tissues (75). Multicolor imaging using single laser 2P excitation has been facilitated by using red LSS-mKate 1 or 2 together with cyan FP due to substantial overlap between their 2P excitation spectra (22). The use of nuclear localized LSS-mKate1 and Golgi-targeted ECFP has enabled the study at subcellular resolution of the motility and Golgi-nucleus alignment of tumor cells as a function of their distance from blood vessels in living mice (Figure 2C). These experiments have shown that breast cancer cells significantly polarize toward vessels within 40 μm, although this polarization drops off rapidly with distance from the blood vessel, implying that the local tumor microenvironments can differentially influence cell invasion and migration.

The LSS-mKate1 and LSS-mKate2 utilized in this study are characterized by high pH stability, photostability, fast chromophore maturation, and monomeric behavior. These features are substantially improved with regard to the other RFP with a large Stokes shift, mKeima, allowing efficient excitation using standard 2P sources. EGFP-mKeima and ECFP-mKeima combinations have also been reported as being suitable for dual-color 2P microscopy (76). Nevertheless, not all fusion proteins with mKeima incorporate well into endogenous cellular structures.

The main challenge for successful intravital imaging is achieving a better signal to noise ratio at greater depth. For the best performance both the excitation and emission maxima of the FP used should lie in the range of 650 to 900 nm, called the "near–infrared optical window" (NIRW) (77). NIRW is characterized by the lowest tissue absorbance. The other thing to consider is the use of an FP with low cytotoxicity (73). The current favorites are E2-Crimson, mNeptune, eqFP650, and monomeric far-red TagRFP657. Further development of bright and even more far-red shifted FP variants remains the main goal for achieving progress in whole-body imaging. The recently described non-GFP-like phytochrome-based FPs are a promising starting point for future development of new probes for this technique (78). Compared with conventional GFP-like proteins, engineering of a bright far-red LSS FP variant seems a straightforward way to achieve better quality of 2P microscopy for intravital imaging.

Advances in FRET imaging: Photochromic FRET

A widespread method to test for protein-protein interactions involves the use of FRET (reviewed in 9,79). In addition to protein-interaction studies, numerous FRET-based biosensors have been elaborated in recent years to detect biologically relevant stimuli such as protease and kinase activity, and ion flux change to name a few (4). However, accurate FRET detection still remains a laborious task (79–81).

A newly devised approach, termed photochromic FRET (pcFRET), allows for accurate and repeated intracellular FRET measurement. pcFRET is based on the optical modulation of acceptor absorbance, thus providing an internal control which thereby eliminates the need for external correction (82). Until recently, pcFRET had been demonstrated only

with photoswitchable chemical dyes (82). The reversibly photoswitchable rsCherryRev and rsCherry FPs suffer from some drawbacks when it comes to their use in pcFRET. Both FPs have complex phototransition behavior, changing the quantum yield rather than the absorbance spectrum upon light illumination (15). They also possess limited brightness and low fluorescence contrast. The recently developed red photoswitchable rsTagRFP, in combination with EYFP as a donor, demonstrated a high potential for the identification of subcellular protein interaction using pcFRET (18). rsTagRFP possesses high-molecular brightness and fluorescence contrast with different absorbance spectra in ON and OFF states. Owing to these attractive features, rsTagRFP has been used to monitor the interaction between epidermal growth factor receptor (EGFR) and growth factor receptor binding protein 2 (Grb2) in live cells by means of pcFRET with EYFP as a donor (Figure 2D, (18)). Using pcFRET, EGFR-Grb2 interactions could be detected in the same cells at different time points, both before and after EGF stimulation. Maximal pcFRET efficiency could be achieved in less than 2 min following EGF addition and remained unchanged for at least 30 min, being the same in both the plasma membrane and in the endosomal compartment. Thus, it was confirmed that EGFR-Grb2 complexes persist through the late stages of endocytosis. It is worthwhile to note that the pcFRET approach requires only a digital imaging wide-field microscope or standard confocal microscope, although FRET accuracy is increased by multiple repetitions of FRET measurements. The low intensity switching ON blue light and moderate intensity switching OFF yellow light in the case of rsTagRFP has been shown to be nonphototoxic for live cells. In addition, the Forster radius of the EYFP-rsTagRFP pair with rsTagRFP in the ON state is comparable to that of the popular ECFP-EYFP and mCerulean-mVenus FRET pairs, enabling detection of protein-protein interaction.

Introduction of other FP-based probes with superior brightness and maturation properties has also advanced FRET applications. For example, the recently developed cyan FPs mTurquoise (83) and Cerulean3 (84) are better choices for FRET applications than conventional CFP. Variants of FP-based probes with improved brightness and photostability should facilitate more sensitive FRET analysis and allow extended imaging.

Currently, one of the most interesting and challenging tasks in FRET imaging is a multiparameter FRET, where two or even three FP-based FRET biosensors are used in the same cell. But the spectral properties of many current FRET pairs preclude their parallel detection in a single cell due to the substantial overlap of excitation and emission spectra. Practical approaches have been used to reach this goal, including: intensiometric instead of the more reliable and commonly used ratiometric approach, spatial separation of sensors, and fluorescence lifetime imaging microscopy utilizing FRET pairs suboptimal for ratiometric imaging (85). Application of linear unmixing techniques has been shown to improve the performance of dual FRET (86–88). The linear unmixing approach is based on the assumption that the emission signal measured in a particular cellular location is linearly proportional to the sum of signals from each probe, allowing the spectral separation of multiple fluorophores (88). However, the use of more spectrally separated biosensors, even with linear unmixing, is preferable since it leads to more accurate and precise imaging.

Better spectral separation of FRET pairs has been achieved, however, this could be further improved by the development of new spectral variants of FPs. Examples of new FPs that have enabled successful dual biosensor FRET include blue FP Sirius (87) and yellow LSS FP mAmetrine (19). The future development of bright orange and red-shifted LSS FPs is a possible way to expand the range of FRET pairs for multiparameter applications.

Conclusions

Currently, monomeric FPs exhibiting complex photochemical behavior such as photoactivation or large Stokes shift are available in green and red colors only. Continuing progress in optical microscopy methods and fluorescence imaging approaches require probes that possess new colors and properties. FP variants with colors distinct from those of the existing probes will facilitate multicolor microscopy. Analysis of the mechanisms of FP chromophore formation and transformation described in this review suggests that fluorescent probes with novel photochemical properties can be designed on the basis of existing conventional FPs. We anticipate that several types of FPs that spectrally complement green and red proteins will be developed in the near future. These include monomeric photoactivatable blue, orange, and far-red FPs as well as monomeric FPs with large Stokes shifted fluorescence in orange and far-red wavelength range. In addition, enhanced monomeric far-red and near-infrared FPs excitable with conventional red lasers and spectrally distinguishable from existing FPs are very desirable for in vivo imaging. Such an expanded future collection of advanced, genetically encoded fluorescent probes will allow their use in numerous multicolor applications.

Acknowledgments

This work was supported by the GM073913 and CA164468 grants from the US National Institutes of Health (both to V.V.V.), by the contract 02.740.11.5141 from the RF Ministry of Education and Science, by the MCB RAS grant (both to K.K.T.), and by the MK-1181.2010.4 grant from the president of the RF (to O.V.S.).

Competing interests

The authors declare no competing interests.

References

1. Wang, Y., J.Y. Shyy, and S. Chien. 2008. Fluorescence proteins, live-cell imaging, and

mechanobiology: seeing is believing. Annu Rev Biomed Eng 10:1-38.
2. Pakhomov, A.A. and V.I. Martynov. 2008. GFP family: structural insights into spectral tuning. Chem Biol 15:755-764.
3. Wu, B., K.D. Piatkevich, T. Lionnet, R.H. Singer, and V.V. Verkhusha. 2011. Modern fluorescent proteins and imaging technologies to study gene expression, nuclear localization, and dynamics. Curr Opin Cell Biol.
4. Frommer, W.B., M.W. Davidson, and R.E. Campbell. 2009. Genetically encoded biosensors based on engineered fluorescent proteins. Chem Soc Rev 38:2833-2841.
5. Heim, R., D.C. Prasher, and R.Y. Tsien. 1994. Wavelength mutations and posttranslational autoxidation of green fluorescent protein. Proc Natl Acad Sci U S A 91:12501-12504.
6. Remington, S.J. 2006. Fluorescent proteins: maturation, photochemistry and photophysics. Curr Opin Struct Biol 16:714-721.
7. Chudakov, D.M., M.V. Matz, S. Lukyanov, and K.A. Lukyanov. 2010. Fluorescent proteins and their applications in imaging living cells and tissues. Physiol Rev 90:1103-1163.
8. Day, R.N. and M.W. Davidson. 2009. The fluorescent protein palette: tools for cellular imaging. Chem Soc Rev 38:2887-2921.
9. Ibraheem, A. and R.E. Campbell. 2010. Designs and applications of fluorescent protein-based biosensors. Curr Opin Chem Biol 14:30-36.
10. Baird, G.S., D.A. Zacharias, and R.Y. Tsien. 1999. Circular permutation and receptor insertion within green fluorescent proteins. Proc Natl Acad Sci U S A 96:11241-11246.
11. Bizzarri, R., M. Serresi, S. Luin, and F. Beltram. 2009. Green fluorescent protein based pH indicators for in vivo use: a review. Anal Bioanal Chem 393:1107-1122.
12. Hanson, G.T., R. Aggeler, D. Oglesbee, M. Cannon, R.A. Capaldi, R.Y. Tsien, and S.J. Remington. 2004. Investigating mitochondrial redox potential with redox-sensitive green fluorescent protein indicators. J Biol Chem 279:13044-13053.
13. Mizuno, T., K. Murao, Y. Tanabe, M. Oda, and T. Tanaka. 2007. Metal-ion-dependent GFP emission in vivo by combining a circularly permutated green fluorescent protein with an engineered metal-ion-binding coiled-coil. J Am Chem Soc 129:11378-11383.
14. Souslova, E.A., V.V. Belousov, J.G. Lock, S. Stromblad, S. Kasparov, A.P. Bolshakov, V.G. Pinelis, Y.A. Labas, et al. 2007. Single fluorescent protein-based Ca2+ sensors with increased dynamic range. BMC Biotechnol 7:37.
15. Subach, F.V., G.H. Patterson, S. Manley, J.M. Gillette, J. Lippincott-Schwartz, and V.V. Verkhusha. 2009. Photoactivatable mCherry for high-resolution two-color fluorescence microscopy. Nat Methods 6:153-159.
16. Subach, F.V., G.H. Patterson, M. Renz, J. Lippincott-Schwartz, and V.V. Verkhusha. 2010. Bright monomeric photoactivatable red fluorescent protein for two-color super-resolution sptPALM of live cells. J Am Chem Soc 132:6481-6491.
17. Kogure, T., S. Karasawa, T. Araki, K. Saito, M. Kinjo, and A. Miyawaki. 2006. A fluorescent variant of a protein from the stony coral Montipora facilitates dual-color single-laser fluorescence cross-correlation spectroscopy. Nat Biotechnol 24:577-581.
18. Subach, F.V., L. Zhang, T.W. Gadella, N.G. Gurskaya, K.A. Lukyanov, and V.V. Verkhusha. 2010. Red fluorescent protein with reversibly photoswitchable absorbance for photochromic FRET. Chem Biol 17:745-755.
19. Ai, H.W., K.L. Hazelwood, M.W. Davidson, and R.E. Campbell. 2008. Fluorescent protein FRET pairs for ratiometric imaging of dual biosensors. Nat Methods 5:401-403.
20. Shcherbo, D., Shemiakina, II, A.V. Ryabova, K.E. Luker, B.T. Schmidt, E.A. Souslova, T.V. Gorodnicheva, L. Strukova, et al. 2010. Near-infrared fluorescent proteins. Nat Methods 7:827-829.
21. Lin, M.Z., M.R. McKeown, H.L. Ng, T.A. Aguilera, N.C. Shaner, R.E. Campbell, S.R. Adams, L.A. Gross, et al. 2009. Autofluorescent proteins with excitation in the optical window for intravital imaging in mammals. Chem Biol 16:1169-1179.
22. Piatkevich, K.D., J. Hulit, O.M. Subach, B. Wu, A. Abdulla, J.E. Segall, and V.V. Verkhusha. 2010. Monomeric red fluorescent proteins with a large Stokes shift. Proc Natl Acad Sci U S A 107:5369-5374.
23. Barondeau, D.P., C.J. Kassmann, J.A. Tainer, and E.D. Getzoff. 2006. Understanding GFP posttranslational chemistry: structures of designed variants that achieve backbone fragmentation, hydrolysis, and decarboxylation. J Am Chem Soc 128:4685-4693.
24. Barondeau, D.P., C.J. Kassmann, J.A. Tainer, and E.D. Getzoff. 2007. The case of the missing ring: radical cleavage of a carbon-carbon bond and implications for GFP chromophore biosynthesis. J Am Chem Soc 129:3118-3126.
25. Wachter, R.M., J.L. Watkins, and H. Kim. 2010. Mechanistic diversity of red fluorescence acquisition by GFP-like proteins. Biochemistry 49:7417-7427.
26. Ehrig, T., D.J. O'Kane, and F.G. Prendergast. 1995. Green-fluorescent protein mutants with altered fluorescence excitation spectra. FEBS Lett 367:163-166.
27. Heim, R., A.B. Cubitt, and R.Y. Tsien. 1995. Improved green fluorescence. Nature 373:663-664.
28. Zapata-Hommer, O. and O. Griesbeck. 2003. Efficiently folding and circularly permuted variants of the Sapphire mutant of GFP. BMC Biotechnol 3:5.
29. Henderson, J.N., M.F. Osborn, N. Koon, R. Gepshtein, D. Huppert, and S.J. Remington. 2009. Excited state proton transfer in the red fluorescent protein mKeima. J Am Chem Soc 131:13212-13213.
30. Piatkevich, K.D., V.N. Malashkevich, S.C. Almo, and V.V. Verkhusha. 2010. Engineering ESPT pathways based on structural analysis of LSSmKate red fluorescent proteins with large Stokes shift. J Am Chem Soc 132:10762-10770.
31. Shi, X., P. Abbyad, X. Shu, K. Kallio, P. Kanchanawong, W. Childs, S.J. Remington, and S.G. Boxer. 2007. Ultrafast excited-state dynamics in the green fluorescent protein variant S65T/H148D. 2. Unusual photophysical properties. Biochemistry 46:12014-12025.
32. Shu, X., K. Kallio, X. Shi, P. Abbyad, P. Kanchanawong, W. Childs, S.G. Boxer, and S.J. Remington. 2007. Ultrafast excited-state dynamics in the green fluorescent protein

variant S65T/H148D. 1. Mutagenesis and structural studies. Biochemistry 46:12005-12013.
33. Yarbrough, D., R.M. Wachter, K. Kallio, M.V. Matz, and S.J. Remington. 2001. Refined crystal structure of DsRed, a red fluorescent protein from coral, at 2.0-A resolution. Proc Natl Acad Sci U S A 98:462-467.
34. Gross, L.A., G.S. Baird, R.C. Hoffman, K.K. Baldridge, and R.Y. Tsien. 2000. The structure of the chromophore within DsRed, a red fluorescent protein from coral. Proc Natl Acad Sci U S A 97:11990-11995.
35. Pletnev, S., F.V. Subach, Z. Dauter, A. Wlodawer, and V.V. Verkhusha. 2010. Understanding blue-to-red conversion in monomeric fluorescent timers and hydrolytic degradation of their chromophores. J Am Chem Soc 132:2243-2253.
36. Strack, R.L., D.E. Strongin, L. Mets, B.S. Glick, and R.J. Keenan. 2010. Chromophore formation in DsRed occurs by a branched pathway. J Am Chem Soc 132:8496-8505.
37. Subach, O.M., V.N. Malashkevich, W.D. Zencheck, K.S. Morozova, K.D. Piatkevich, S.C. Almo, and V.V. Verkhusha. 2010. Structural characterization of acylimine-containing blue and red chromophores in mTagBFP and TagRFP fluorescent proteins. Chem Biol 17:333-341.
38. Subach, F.V., O.M. Subach, I.S. Gundorov, K.S. Morozova, K.D. Piatkevich, A.M. Cuervo, and V.V. Verkhusha. 2009. Monomeric fluorescent timers that change color from blue to red report on cellular trafficking. Nat Chem Biol 5:118-126.
39. van Thor, J.J., T. Gensch, K.J. Hellingwerf, and L.N. Johnson. 2002. Phototransformation of green fluorescent protein with UV and visible light leads to decarboxylation of glutamate 222. Nat Struct Biol 9:37-41.
40. Patterson, G.H. and J. Lippincott-Schwartz. 2002. A photoactivatable GFP for selective photolabeling of proteins and cells. Science 297:1873-1877.
41. Chudakov, D.M., V.V. Verkhusha, D.B. Staroverov, E.A. Souslova, S. Lukyanov, and K.A. Lukyanov. 2004. Photoswitchable cyan fluorescent protein for protein tracking. Nat Biotechnol 22:1435-1439.
42. Henderson, J.N., R. Gepshtein, J.R. Heenan, K. Kallio, D. Huppert, and S.J. Remington. 2009. Structure and mechanism of the photoactivatable green fluorescent protein. J Am Chem Soc 131:4176-4177.
43. Mizuno, H., T.K. Mal, K.I. Tong, R. Ando, T. Furuta, M. Ikura, and A. Miyawaki. 2003. Photo-induced peptide cleavage in the green-to-red conversion of a fluorescent protein. Mol Cell 12:1051-1058.
44. Ando, R., H. Hama, M. Yamamoto-Hino, H. Mizuno, and A. Miyawaki. 2002. An optical marker based on the UV-induced green-to-red photoconversion of a fluorescent protein. Proc Natl Acad Sci U S A 99:12651-12656.
45. Bogdanov, A.M., A.S. Mishin, I.V. Yampolsky, V.V. Belousov, D.M. Chudakov, F.V. Subach, V.V. Verkhusha, S. Lukyanov, and K.A. Lukyanov. 2009. Green fluorescent proteins are light-induced electron donors. Nat Chem Biol 5:459-461.
46. Piatkevich, K.D. and V.V. Verkhusha. 2010. Advances in engineering of fluorescent proteins and photoactivatable proteins with red emission. Curr Opin Chem Biol 14:23-29.
47. Henderson, J.N., H.W. Ai, R.E. Campbell, and S.J. Remington. 2007. Structural basis for reversible photobleaching of a green fluorescent protein homologue. Proc Natl Acad Sci U S A 104:6672-6677.
48. Adam, V., M. Lelimousin, S. Boehme, G. Desfonds, K. Nienhaus, M.J. Field, J. Wiedenmann, S. McSweeney, et al. 2008. Structural characterization of IrisFP, an optical highlighter undergoing multiple photo-induced transformations. Proc Natl Acad Sci U S A 105:18343-18348.
49. Schafer, L.V., G. Groenhof, M. Boggio-Pasqua, M.A. Robb, and H. Grubmuller. 2008. Chromophore protonation state controls photoswitching of the fluoroprotein asFP595. PLoS Comput Biol 4:e1000034.
50. Remington, S.J., R.M. Wachter, D.K. Yarbrough, B. Branchaud, D.C. Anderson, K. Kallio, and K.A. Lukyanov. 2005. zFP538, a yellow-fluorescent protein from Zoanthus, contains a novel three-ring chromophore. Biochemistry 44:202-212.
51. Shu, X., N.C. Shaner, C.A. Yarbrough, R.Y. Tsien, and S.J. Remington. 2006. Novel chromophores and buried charges control color in mFruits. Biochemistry 45:9639-9647.
52. Fernandez-Suarez, M. and A.Y. Ting. 2008. Fluorescent probes for super-resolution imaging in living cells. Nat Rev Mol Cell Biol 9:929-943.
53. Ji, N., H. Shroff, H. Zhong, and E. Betzig. 2008. Advances in the speed and resolution of light microscopy. Curr Opin Neurobiol 18:605-616.
54. Buckers, J., D. Wildanger, G. Vicidomini, L. Kastrup, and S.W. Hell. 2011. Simultaneous multi-lifetime multi-color STED imaging for colocalization analyses. Opt Express 19:3130-3143.
55. Bretschneider, S., C. Eggeling, and S.W. Hell. 2007. Breaking the diffraction barrier in fluorescence microscopy by optical shelving. Phys Rev Lett 98:218103.
56. Kner, P., B.B. Chhun, E.R. Griffis, L. Winoto, and M.G. Gustafsson. 2009. Super-resolution video microscopy of live cells by structured illumination. Nat Methods 6:339-342.
57. Huang, B., W. Wang, M. Bates, and X. Zhuang. 2008. Three-dimensional super-resolution imaging by stochastic optical reconstruction microscopy. Science 319:810-813.
58. Betzig, E., G.H. Patterson, R. Sougrat, O.W. Lindwasser, S. Olenych, J.S. Bonifacino, M.W. Davidson, J. Lippincott-Schwartz, and H.F. Hess. 2006. Imaging intracellular fluorescent proteins at nanometer resolution. Science 313:1642-1645.
59. Patterson, G., M. Davidson, S. Manley, and J. Lippincott-Schwartz. 2010. Superresolution imaging using single-molecule localization. Annu Rev Phys Chem 61:345-367.
60. Greenfield, D., A.L. McEvoy, H. Shroff, G.E. Crooks, N.S. Wingreen, E. Betzig, and J. Liphardt. 2009. Self-organization of the Escherichia coli chemotaxis network imaged with super-resolution light microscopy. PLoS Biol 7:e1000137.
61. Hess, S.T., T.J. Gould, M.V. Gudheti, S.A. Maas, K.D. Mills, and J. Zimmerberg. 2007. Dynamic clustered distribution of hemagglutinin resolved at 40 nm in living cell membranes discriminates between raft theories. Proc Natl Acad Sci U S A 104:17370-17375.
62. Manley, S., J.M. Gillette, G.H. Patterson, H. Shroff, H.F. Hess, E. Betzig, and J. Lippincott-Schwartz. 2008. High-density mapping

of single-molecule trajectories with photoactivated localization microscopy. Nat Methods 5:155-157.
63. Niu, L. and J. Yu. 2008. Investigating intracellular dynamics of FtsZ cytoskeleton with photoactivation single-molecule tracking. Biophys J 95:2009-2016.
64. Frost, N.A., H. Shroff, H. Kong, E. Betzig, and T.A. Blanpied. 2010. Single-molecule discrimination of discrete perisynaptic and distributed sites of actin filament assembly within dendritic spines. Neuron 67:86-99.
65. Schermelleh, L., P.M. Carlton, S. Haase, L. Shao, L. Winoto, P. Kner, B. Burke, M.C. Cardoso, et al. 2008. Subdiffraction multicolor imaging of the nuclear periphery with 3D structured illumination microscopy. Science 320:1332-1336.
66. Baddeley, D., V.O. Chagin, L. Schermelleh, S. Martin, A. Pombo, P.M. Carlton, A. Gahl, P. Domaing, et al. 2010. Measurement of replication structures at the nanometer scale using super-resolution light microscopy. Nucleic Acids Res 38:e8.
67. Hoopmann, P., A. Punge, S.V. Barysch, V. Westphal, J. Buckers, F. Opazo, I. Bethani, M.A. Lauterbach, et al. 2010. Endosomal sorting of readily releasable synaptic vesicles. Proc Natl Acad Sci U S A 107:19055-19060.
68. Morozova, K.S., K.D. Piatkevich, T.J. Gould, J. Zhang, J. Bewersdorf, and V.V. Verkhusha. 2010. Far-red fluorescent protein excitable with red lasers for flow cytometry and superresolution STED nanoscopy. Biophys J 99:L13-15.
69. Hein, B., K.I. Willig, and S.W. Hell. 2008. Stimulated emission depletion (STED) nanoscopy of a fluorescent protein-labeled organelle inside a living cell. Proc Natl Acad Sci U S A 105:14271-14276.
70. Shroff, H., C.G. Galbraith, J.A. Galbraith, H. White, J. Gillette, S. Olenych, M.W. Davidson and E. Betzig. 2007. Dual-color superresolution imaging of genetically expressed probes within individual adhesion complexes. Proc Natl Acad Sci U S A 104:20308-20313.
71. Huang, B. 2010. Super-resolution optical microscopy: multiple choices. Curr Opin Chem Biol 14:10-14.
72. Schermelleh, L., R. Heintzmann, and H. Leonhardt. 2010. A guide to super-resolution fluorescence microscopy. J Cell Biol 190:165-175.
73. Strack, R.L., B. Hein, D. Bhattacharyya, S.W. Hell, R.J. Keenan, and B.S. Glick. 2009. A rapidly maturing far-red derivative of DsRed-Express2 for whole-cell labeling. Biochemistry 48:8279-8281.
74. Denk, W., J.H. Strickler, and W.W. Webb. 1990. Two-photon laser scanning fluorescence microscopy. Science 248:73-76.
75. Zipfel, W.R., R.M. Williams, and W.W. Webb. 2003. Nonlinear magic: multiphoton microscopy in the biosciences. Nat Biotechnol 21:1369-1377.
76. Kogure, T., H. Kawano, Y. Abe, and A. Miyawaki. 2008. Fluorescence imaging using a fluorescent protein with a large Stokes shift. Methods 45:223-226.
77. Jobsis, F.F. 1977. Noninvasive, infrared monitoring of cerebral and myocardial oxygen sufficiency and circulatory parameters. Science 198:1264-1267.
78. Shu, X., A. Royant, M.Z. Lin, T.A. Aguilera, V. Lev-Ram, P.A. Steinbach, and R.Y. Tsien. 2009. Mammalian expression of infrared fluorescent proteins engineered from a bacterial phytochrome. Science 324:804-807.
79. Piston, D.W. and G.J. Kremers. 2007. Fluorescent protein FRET: the good, the bad and the ugly. Trends Biochem Sci 32:407-414.
80. Jares-Erijman, E.A. and T.M. Jovin. 2006. Imaging molecular interactions in living cells by FRET microscopy. Curr Opin Chem Biol 10:409-416.
81. Sinnecker, D., P. Voigt, N. Hellwig, and M. Schaefer. 2005. Reversible photobleaching of enhanced green fluorescent proteins. Biochemistry 44:7085-7094.
82. Mao, S., R.K. Benninger, Y. Yan, C. Petchprayoon, D. Jackson, C.J. Easley, D.W. Piston, and G. Marriott. 2008. Optical lock-in detection of FRET using synthetic and genetically encoded optical switches. Biophys J 94:4515-4524.
83. Goedhart, J., L. van Weeren, M.A. Hink, N.O. Vischer, K. Jalink, and T.W. Gadella, Jr. 2010. Bright cyan fluorescent protein variants identified by fluorescence lifetime screening. Nat Methods 7:137-139.
84. Markwardt, M.L., G.J. Kremers, C.A. Kraft, K. Ray, P.J. Cranfill, K.A. Wilson, R.N. Day, R.M. Wachter, et al. 2011. An improved cerulean fluorescent protein with enhanced brightness and reduced reversible photoswitching. PLoS One 6:e17896.
85. Carlson, H.J. and R.E. Campbell. 2009. Genetically encoded FRET-based biosensors for multiparameter fluorescence imaging. Curr Opin Biotechnol 20:19-27.
86. Niino, Y., K. Hotta, and K. Oka. 2009. Simultaneous live cell imaging using dual FRET sensors with a single excitation light. PLoS One 4:e6036.
87. Tomosugi, W., T. Matsuda, T. Tani, T. Nemoto, I. Kotera, K. Saito, K. Horikawa, and T. Nagai. 2009. An ultramarine fluorescent protein with increased photostability and pH insensitivity. Nat Methods 6:351-353.
88. Ecker, R.C., R. de Martin, G.E. Steiner, and J.A. Schmid. 2004. Application of spectral imaging microscopy in cytomics and fluorescence resonance energy transfer (FRET) analysis. Cytometry A 59:172-181.

Received 30 June 2011; accepted: 29 September 2011.

Address correspondence to Vladislav V. Verkhusha, Department of Anatomy and Structural Biology and Gruss-Lipper Biophotonics Center, Albert Einstein College of Medicine, Bronx, NY 10461, USA. e-mail: vladislav.verkhusha@einstein.yu.edu